Formation of antiwaves in gap-junction-coupled chains of neurons

Alexander Urban
Department of Physics, University of Pittsburgh,100 Allen Hall, 3941 O'Hara Street, Pittsburgh, Pennsylvania 15260, USA

Bard Ermentrout
Department of Mathematics, University of Pittsburgh, 139 University Place, Pittsburgh, Pennsylvania 15260, USA

(Received 13 March 2012; revised manuscript received 17 May 2012; published 10 July 2012)

Using network models consisting of gap-junction-coupled Wang-Buszaki neurons, we demonstrate that it is possible to obtain not only synchronous activity between neurons but also a variety of constant phase shifts between 0 and π. We call these phase shifts *intermediate stable phase-locked states*. These phase shifts can produce a large variety of wavelike activity patterns in one-dimensional chains and two-dimensional arrays of neurons, which can be studied by reducing the system of equations to a phase model. The 2π periodic coupling functions of these models are characterized by prominent higher order terms in their Fourier expansion, which can be varied by changing model parameters. We study how the relative contribution of the odd and even terms affects what solutions are possible, the basin of attraction of those solutions, and their stability. These models may be applicable to the spinal central pattern generators of the dogfish and also to the developing neocortex of the neonatal rat.

DOI: 10.1103/PhysRevE.86.011907 PACS number(s): 87.19.lj, 05.45.Xt, 87.19.lp

I. INTRODUCTION

In the past few decades, neuroscientists have discovered the importance of oscillations in the brain. Oscillations occur in many neural networks and play key roles in sensory as well as motor systems [1,2]. On the smallest scale of the nervous system, individual neurons can behave as complex nonlinear oscillators [3]. On a larger scale, oscillatory patterns in electroencephalographic (EEG) recordings have been shown to correspond to different cognitive states [3]. Phase oscillator models (obtained from systems of weakly coupled oscillators) have proven extremely useful in the analysis of such systems [4,5].

A pair of symmetric weakly coupled oscillators always has at least two possible periodic (phase-locked) states: the synchronous state and the antiphase state (where they are a half a cycle out of phase). Suppose that for some range of parameters the synchronous solution is stable and, as one of these parameters is varied, the synchronous solution loses stability. In a symmetrically coupled system the synchronous solution generically loses stability in a pitchfork bifurcation. When this pitchfork bifurcation is supercritical it gives rise to two new stable phase-locked solutions in which the phase difference between oscillators is some constant between 0 and π. We refer to such solutions as *intermediate stable phase-locked states*. Intermediate stable phase-locked states between pairs of neurons can be produced in a variety of neuron models by using a variety of coupling schemes as well as by adjusting the parameters which affect the excitability of individual neurons [6–8]. The first work examining this behavior in conductance-based models was by Vanvreeswijk *et al*. [8]. In this paper, the authors studied integrate-and-fire as well as Hodgkin-Huxley neurons. Cymbalyuk has both modeled and experimentally demonstrated an intermediate stable phase-locked state in a system of two "silicon neurons" [9,10]. These intermediate phase-locked states can lead to wavelike behavior in large networks.

Wave activity is ubiquitous in the brain. Traveling waves of electrical activity in the brains of animals have been observed in a variety of species and occur in a diverse set of structures. These structures include the retina, olfactory cortex [11], perigeniculate nucleus [12], neocortex [13], and spinal cord [1], among others [11–15]. In phase models, waves correspond to constant nonzero phase differences between successive pairs of oscillators. There are many ways to generate such phase differences (see Ref. [16], Sec. 8.3.5) such as a gradient in natural frequencies [4], pacemakers, or manipulation of the boundary conditions [17]. For instance, Bressloff *et al*. extended the analysis in Ref. [8] to demonstrate that such phase shifts would arise in a ring of symmetrically coupled integrate-and-fire neurons with delays [18]. In some swimming organisms, it is very important that a fixed phase lag be maintained over a wide range of frequencies. For example, in the lamprey, the lag is about $2\pi/100$ [4], while for the crayfish it is $2\pi/4$ [19]. As we will show in this paper, intermediate stable phase-locked states provide a simple way to produce waves with a stable fixed interoscillator phase difference.

The paper is organized as follows. We first show that by varying the excitability of gap-junction-coupled Wang-Buszaki neurons, we can produce intermediate stable phase-locked states. We then explore the consequences of these states in one-dimensional nearest-neighbor coupled chains. We prove the existence and stability of a wide variety of complex waves including traveling waves and antiwaves. We then study two-dimensional arrays and find two-dimensional analogs of antiwaves and traveling waves.

II. GAP-JUNCTION COUPLING BETWEEN PAIRS OF WANG-BUSZAKI NEURONS

A. Measuring the phase difference between spiking neurons

The Wang-Buszaki model is a conductance based neuron model derived from the Hodgkin-Huxley model. It was originally used to describe fast spiking interneurons in the hippocampus [20]. In this section we examine pairs of Wang-Buszaki neurons reciprocally coupled with gap junctions

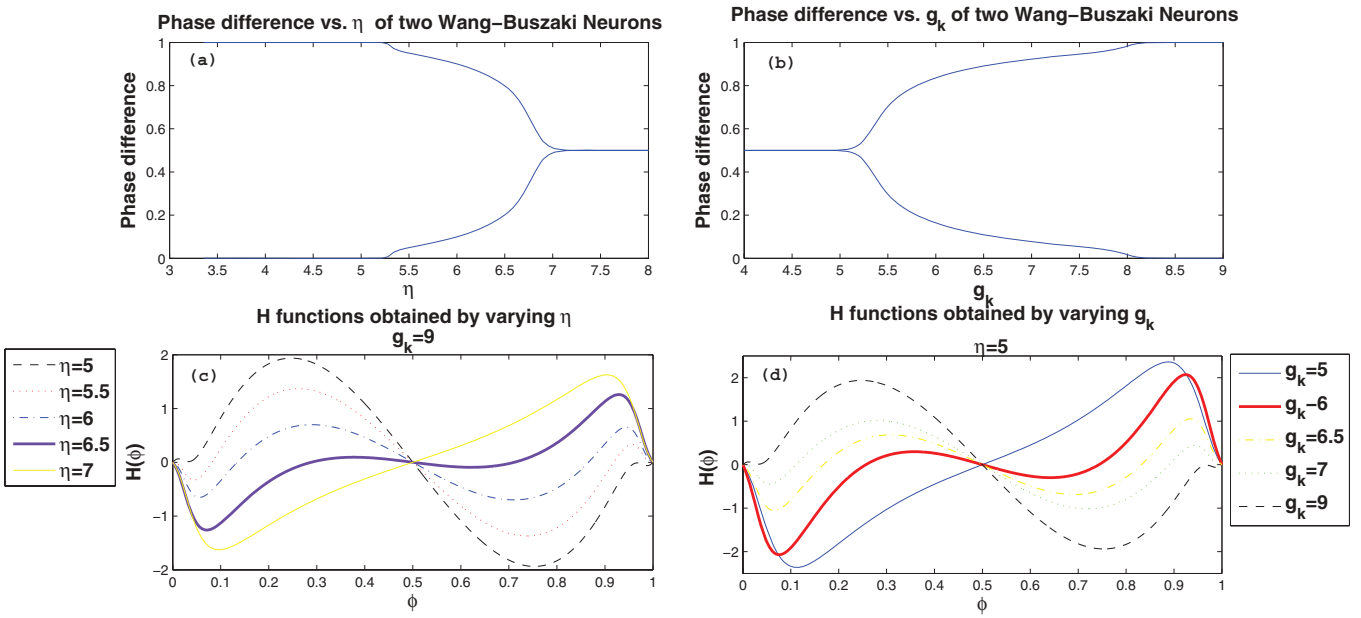

FIG. 1. (Color online) (a) The phase difference between two Wang-Buszaki neurons (full model) as a function of the parameter η. The diagram clearly illustrates a pitchfork bifurcation connecting the synchronous and antiphase solutions. (b) Plot of the phase difference for varying values of g_{K}. (c) Plot of the odd part of the interaction function [cf. Eqs. (8) and (9)] for different values of η (the dimensionless temperature-dependent time constant). (d) Calculation of the odd part of the interaction function for different values of g_{K}. The zeros of these functions correspond to the stable phase-locked solutions.

and ask what happens as we vary parameters which affect the excitability of the individual cells. Gap junctions are specialized ion channels connecting the cytoplasm of the presynaptic and postsynaptic cell. A depolarizing ionic current is driven by the potential difference between the cells. In order to understand the role that gap junctions play in rhythmically oscillating networks, consider just two neurons coupled with gap junctions. The coupled neuron equations will have the following form:

$$\begin{aligned} C\dot{V}_1 &= -I_{\mathrm{Na}} - I_{\mathrm{K}} - I_L + I_0 + g(V_2 - V_1) \\ C\dot{V}_2 &= -I_{\mathrm{Na}} - I_{\mathrm{K}} - I_L + I_0 + g(V_1 - V_2). \end{aligned} \tag{1}$$

These currents are given by the equations

$$\begin{aligned} I_{\mathrm{Na}} &= g_{\mathrm{Na}} m_\infty^3 h(V - V_{\mathrm{Na}}), \\ I_{\mathrm{K}} &= g_{\mathrm{K}} n^4 (V - V_{\mathrm{K}}), \\ I_L &= g_L (V - V_L). \end{aligned} \tag{2}$$

C is the the membrane capacitance measured in units of $\mu\mathrm{F/cm}^2$. The parameters V_{Na}, V_{K} and V_L are the reversal potentials for the ion channels. The parameters g, g_{Na}, g_{K}, and g_L are constants describing the conductances of their respectively labeled ion channels. Typically, they are measured in units of $\mathrm{mS/cm}^2$. The m and the h are the time-dependent activation and deactivation variables which are described by the equations

$$\begin{aligned} \frac{dh}{dt} &= \eta[\alpha_h(V)(1-h) - \beta_h(V)h], \\ \frac{dm}{dt} &= \eta[\alpha_m(V)(1-m) - \beta_m(V)m]. \end{aligned} \tag{3}$$

In these equations, η is an overall channel switching rate determined by the temperature of the system [21]. The nonlinearities $\alpha_i(V)$, $\beta_i(V)$, as well as the parameters used in the simulations, are referenced in the Appendix.

Previously, Pfeuty *et al*. have studied pairs of Wang-Buszaki neurons with gap-junction coupling and shown that by varying the potassium and sodium conductances, one can vary the stability of the synchronous in-phase and antiphase states [22]. In order to find parameter regimes in which intermediate phase-locked states exist, we varied the potassium conductance g_{K} and also the temperature-dependent rate constant η. Parameters such as these play key roles in the behavior of both central pattern generators and large scale oscillatory networks [23,24]. The most important consequence of varying these parameters is that the absolute refractory period decreases. The neuron is less hyperpolarized after the action potential for larger η or smaller g_{K} [22]. In other words, this smaller absolute refractory region allows for the neuron to fire more quickly [22]. Consider the upper half of Fig. 1: Figs. 1(a) and 1(b) are calculations of the phase difference between two Wang-Buszaki neurons computed after 1500 ms of integration time for different values of g_{K} (the maximal potassium conductance) and η (the temperature-dependent time constant). The phase difference ϕ was measured as the difference between the times at which V_1 and V_2 cross zero, with a positive slope divided by the period of the oscillation. Holding the stimulus current constant at $i_0 = 0.63\ \mathrm{nA/cm}^2$ and varying either the parameter η or g_{K}, we are able to demonstrate a supercritical pitchfork bifurcation in the phase difference between neurons. Figure 1(a) illustrates the bifurcation of the system of two neurons from synchrony to antiphase behavior as η is increased. For values of η between 5.0 and 7.0 the system passes through all possible stable

relative phase-locked solutions varying between 0.0 and π. Figure 1(b) is a plot of the phase difference between neurons as we decrease g_K. As we decrease g_K between 8.0 and 5.0 we also obtain intermediate stable phase-locked solutions.

B. Calculation of the interaction function

In order to simplify the analysis, we reduce our system of neurons to a phase model. This can be accomplished by applying Malkin's theorem [2]. Consider two weakly coupled systems (by weak, we mean that the coupling acts to only affect the phase and not the amplitude of the oscillation [2]) of coupled differential equations describing tonically firing neurons:

$$V_1' = F(V_1) + \epsilon C_1(V_1, V_2) + O(\epsilon^2), \tag{4}$$

$$V_2' = F(V_2) + \epsilon C_2(V_2, V_1) + O(\epsilon^2). \tag{5}$$

Then Malkin's theorem states

$$V_1(t) = V_0(\theta_1) + O(\epsilon), \quad V_2(t) = V_0(\theta_2) + O(\epsilon),$$

where V_0 is the solution to the homogenous equation. Furthermore,

$$\frac{d\theta_1}{dt} = 1 + \epsilon H_1(\theta_2 - \theta_1) + O(\epsilon^2), \tag{6}$$

$$\frac{d\theta_2}{dt} = 1 + \epsilon H_2(\theta_1 - \theta_2) + O(\epsilon^2), \tag{7}$$

where

$$H_j(\phi) := \frac{1}{T}\int_0^P V^*(t) \cdot C_j[V_0(t), V_0(t+\phi)]dt. \tag{8}$$

Here V^* is the adjoint of the linearized equation (4). Let $\phi := \theta_2 - \theta_1$. Then

$$\frac{d\phi}{dt} = -2\epsilon H_{\text{odd}}(\phi) := \epsilon[H(-\phi) - H(\phi)]. \tag{9}$$

The right-hand sides of these phase model equations are described by interaction functions which are derived from the full model. Zeros of $H_{\text{odd}}(\phi)$ determine the possible phase-locked states and those for which $H'_{\text{odd}}(\phi) > 0$ are stable.

We calculated the interaction functions for several values of g_K and η. Figures 1(c) and 1(d) show the odd portions of the interaction functions calculated with various parameter values. We write these interaction functions in terms of their Fourier series:

$$H(x) = \frac{a_0}{2} + \sum_{n=1}^{\infty}[a_n \cos(nx) + b_n \sin(nx)]. \tag{10}$$

For example, Table I shows the first few Fourier modes of the interaction function computed from the full model with $\eta = 6$. This table demonstrates the substantial contribution of higher order Fourier terms to the interaction function near the bifurcation point.

Observe that the first two odd Fourier terms in Table I are the dominant ones (b_1,b_2). As the shape of $H_{\text{odd}}(\phi)$ depends only on the odd terms, a_j have no effect on the existence and stability of the locked solutions for a pair of symmetrically coupled oscillators. However, once there are more than just two oscillators, the even terms play an important role, particularly as far as stability is concerned. We find that as η changes between 5 and 7, the Fourier coefficient b_2 remains negative and b_1 goes to zero. For this reason, in the rest of this paper, we will use a truncated version of the H function that contains only three terms:

$$H(x) = b_1 \sin(x) + b_2 \sin(2x) + a_1 \cos(x). \tag{11}$$

Unless otherwise stated, we typically take $b_1 = 1$ and $b_2 = -0.75$, giving zeros of H_{odd} at $\phi = 0, \pi, \pm\cos^{-1}(2/3) \approx \pm 0.847$. We remark that this particular form of $H_{\text{odd}}(\phi)$ arises in the bead on a hoop instability (Ref. [25], Chap. 3.5) and in a model for the coordination of finger tapping [26]. If $b_2 < 0$ is fixed and negative, then as b_1 decreases from a large positive value, the synchronous solution loses stability (at $b_1 = -2b_2$) and a branch of intermediate stable phase-locked solutions bifurcates. This branch remains stable until b_1 becomes sufficiently negative, $b_1 < 2b_2$, whereupon the antiphase solution is stable.

TABLE I. Fourier coefficients of the interaction function, Eq. (8) (computed from the full model with $\eta = 6$). Near the bifurcation point from synchrony there are substantial higher order even and odd Fourier terms.

$a_0 = 5.1974931$	
$a_1 = -2.9970722$	$b_1 = 0.47408548$
$a_2 = -0.92187762$	$b_2 = -0.36833799$
$a_3 = -0.44113794$	$b_3 = -0.2577318$
$a_4 = -0.25482759$	$b_4 = -0.15762125$
$a_5 = -0.16416954$	$b_5 = -0.09083201$
$a_6 = -0.11295291$	$b_6 = -0.048487604$

III. WAVES IN LARGE NETWORKS

This section is a study of wave behavior in both chains and two-dimensional arrays of neurons with nearest-neighbor coupling in regimes where there is an intermediate stable phase-locked state for pairwise coupling. Primarily, we study phase models which use the interaction functions (or approximations of them) derived from the Wang-Buszaki model. Our models may be relevant to patterns of wave activity in the neonatal rat. Peinado *et al.* was able to observe wave activity in gap-junction-coupled interneurons in rat neocortex prior to day 12 of development [13]. Furthermore, he was able to enhance these waves by applying halothane and picrotoxin. Picrotoxin blocks inhibitory synapses while halothane reduces the potassium conductance. In general, he observed that the reduction in potassium directly led to the formation of waves. Since our intermediate stable phase-locked states can occur in gap-junction-coupled neurons by reducing the potassium conductance, this may be experimental evidence that this effect plays a role in wave formation in a two-dimensional network.

We focus on a specific type of solution to the phase equations, known as antiwaves. Antiwaves were first studied in two papers by Ermentrout and Kopell [17,27]. Similar phenomena have been examined by Strogatz *et al.* (uniformly twisted waves) and Blasius *et al.* [one-dimensional (1D)

quasiregular concentric waves] [28–30]. Antiwaves consist of waves either initiated at the ends and colliding in the middle or waves initiating from the middle and terminating at the ends. The latter are, in a sense, equivalent to one-dimensional target patterns. The wave number for these waves (the spatial gradient of the phase) shows an abrupt change of sign, which we will call a kink. Similar phase waves have been demonstrated in mechanical systems [31]. Antiwaves have been experimentally observed in the spinal cords of dogfish [32] and may well be present in other biological tissue. For instance, similar patterns of electrical activity have been observed in the muscle of the colon of a cat [33]. Central pattern generators in the fins of electric fish have also been known to produce antiwaves [27]. These animals are able to produce a variety of complex waves in which the "kink" or lead oscillator in the wave is able to shift [27].

The rest of this paper is organized into several sections. We begin in Sec. III A by discussing the basic phase models and boundary conditions. This is followed by an analysis of both an ordinary traveling wave (Sec. III B) and antiwave solutions (Sec. III C). In Sec. III D, we demonstrate that the probability of obtaining a particular solution depends on the relative contribution of the even component of the interaction function. We show that starting from the antiwave solution, if the even component is sufficiently large, perturbations initiated at one end of the chain can propagate down the chain and shift the position of the kink. Finally, in Sec. V we demonstrate that this analysis can be extended to higher dimensions and that a variety of antiwave patterns are possible in two-dimensional oscillator arrays.

A. Models and boundary conditions

The models we consider were introduced by Kopell and Ermentrout in 1986 [17]. These models primarily describe networks of neurons with nearest-neighbor coupling. In analyzing these equations we apply two types of boundary conditions: periodic boundary conditions and nonreflecting boundary conditions. For a system of $N+1$ neurons with periodic boundary conditions, the system of phase equations may be written

$$\begin{aligned}
\dot{\theta}_1 &= \omega_1 + H_L(\theta_{N+1}-\theta_1) + H_R(\theta_2-\theta_1),\\
\dot{\theta}_2 &= \omega_2 + H_L(\theta_1-\theta_2) + H_R(\theta_3-\theta_2),\\
&\vdots\\
\dot{\theta}_{N+1} &= \omega_{N+1} + H_L(\theta_N-\theta_{N+1}) + H_R(\theta_1-\theta_{N+1}).
\end{aligned} \tag{12}$$

In these equations, the ω_i represents the natural frequencies of the oscillators. We denote the coupling in the two possible directions as $H_L(\phi)$ and $H_R(\phi)$. In general, we assume that the coupling is isotropic, so that $H_R(\phi) = H_L(\phi) = H(\phi)$. Ultimately, we are interested in phase-locking behavior, and thus we make a change in the variables: $\phi_j = \theta_{j+1} - \theta_j$. This results in a system of N phase equations:

$$\begin{aligned}
\dot{\phi}_1 &= \Delta\omega_1 + H(\phi_2) + H(-\phi_1) - H\left(\sum_{j=1}^{N}\phi_j\right) - H(\phi_1),\\
\dot{\phi}_2 &= \Delta\omega_2 + H(\phi_3) + H(-\phi_2) - H(-\phi_1) - H(\phi_2),\\
\dot{\phi}_j &= \Delta\omega_j + H(\phi_{j+1}) + H(-\phi_j) - H(-\phi_{j-1}) - H(\phi_j),\\
&\vdots\\
\dot{\phi}_N &= \Delta\omega_1 + H(-\phi_N) + H\left(-\sum_{j=1}^{N}\phi_j\right)\\
&\quad - H(-\phi_{N-1}) - H(\phi_N).
\end{aligned} \tag{13}$$

In these equations $\Delta\omega_i$ is the frequency gradient between oscillators. In most of our simulations, we assume identical frequencies so $\Delta\omega_i = 0$.

The second type of boundary condition that we use is a variation of what are known as nonreflecting boundary conditions [34]. Nonreflecting boundary conditions are implemented in order to attempt to eliminate reflections and to "trick" the neurons at the ends of the chains, neuron 1 and neuron $N+1$, into behaving as though the chain is infinite. If one were to think of the chain as being a continuous system, then the boundary conditions are simply a statement that $\frac{d\phi(x,t)}{dx} = 0$ when evaluated at the ends of the chain. There is a precedent for using such boundary conditions in nonlinear oscillator problems—for an example, see Ref. [31]. Applying these boundary conditions to our phase equations, we have [35]

$$\begin{aligned}
\theta_0 &= \theta_2,\\
\theta_{N+1} &= \theta_{N-1},
\end{aligned} \tag{14}$$

and our phase equations become

$$\begin{aligned}
\dot{\phi}_1 &= \Delta\omega_1 + H(\phi_2) + H(-\phi_1) - 2H(\phi_1),\\
\dot{\phi}_2 &= \Delta\omega_2 + H(\phi_3) + H(-\phi_2) - H(-\phi_1) - H(\phi_2),\\
\dot{\phi}_j &= \Delta\omega_j + H(\phi_{j+1}) + H(-\phi_j) - H(-\phi_{j-1}) - H(\phi_j),\\
&\vdots\\
\dot{\phi}_N &= \Delta\omega_N + 2H(-\phi_N) - H(-\phi_{N-1}) - H(\phi_N).
\end{aligned} \tag{15}$$

B. Traveling waves in chains of coupled oscillators

The wave solution for the traveling wave can be written

$$\phi_j = j\phi^* + \Delta\omega t, \tag{16}$$

where j is the index of the oscillator and ϕ^* is the phase shift between adjacent oscillators. Substituting this solution into the equations with nonreflecting boundary conditions, we see that (16) is a solution provided that $H(\phi^*) = H(-\phi^*)$. Since our interaction function has both odd and even components, this statement is true only if ϕ^* is the root of $H(\phi)_{\text{odd}}$. Thus, the stable phase-locked states for pairwise symmetrically coupled oscillators determine the wave number ϕ^*. In a continuum limit, we can consider $\theta(x,t)$ to be a function of both position and time. If we take the derivative of $\theta(x,t)$ with respect to t we obtain the expression [17]

$$\frac{d\theta}{dt} + \frac{\partial\theta}{\partial x}\frac{\partial x}{\partial t} = 0, \tag{17}$$

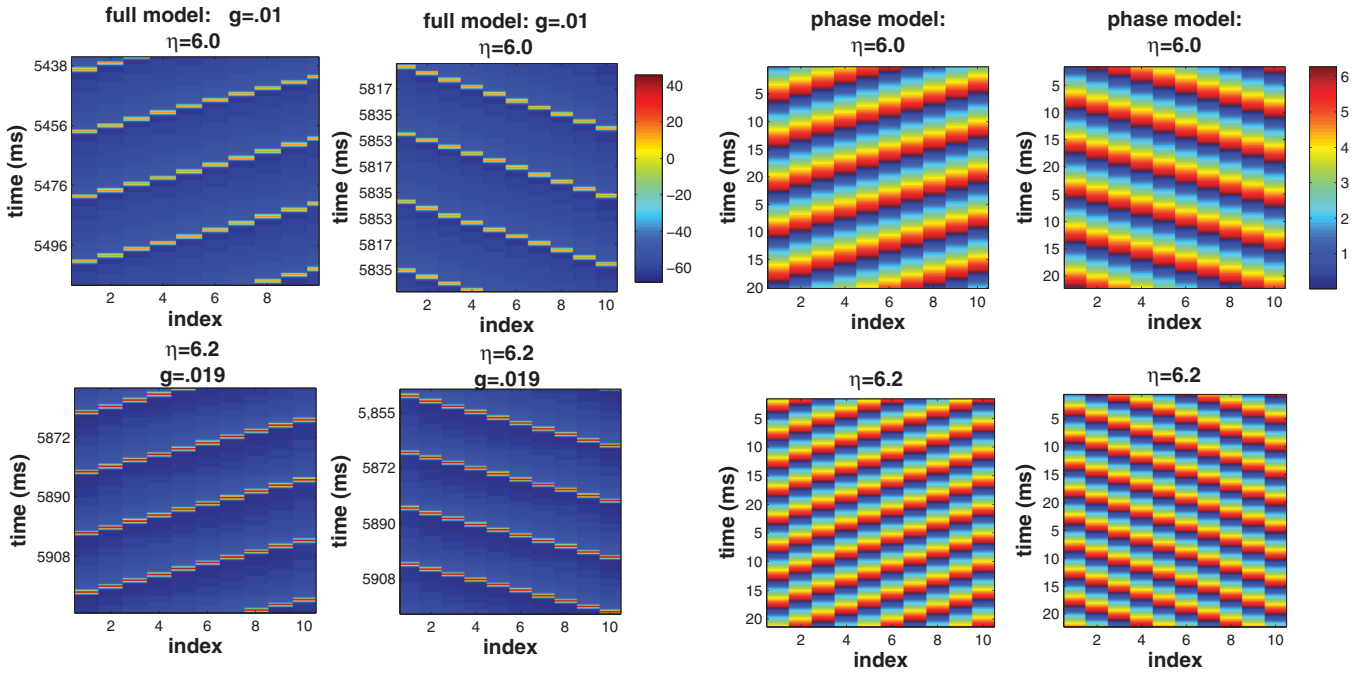

FIG. 2. (Color online) Examples of traveling waves in both the Wang-Buszaki model (left) and the phase model (right) corresponding to two different values of the temperature-dependent time constant η. The phase model reproduces the dynamics of the full model. Furthermore, it is clear from the phase model that as one increases the constant η, the wavelength of the traveling waves decreases. The coupling strength in the full model is small: It must be on the order of $g = 0.01$ mS/cm^2 to ensure phase locking.

which is equivalent to

$$\omega + \phi^* v_\theta = 0, \qquad v_\theta = \frac{\omega}{\phi^*}. \tag{18}$$

This is an expression for the phase velocity of the wave. Therefore, we see that we may identify the wave number of the system as $k = \phi^*$. The stable phase-locked state between pairs of oscillators defines the wave number of a traveling wave. In the last section it was demonstrated that as we vary constants η and g_K in the Wang-Buszaki model, the stable fixed point changes. This translates to a change in wavelength in a chain of neurons. Figure 2 shows a comparison between the phase model and full model for a variety of g_K and η. The four panels on the left correspond to the full model. The panels on the right correspond to the phase model. The phase model quantitatively reproduces the dynamics of the full model. The phase model clearly demonstrates that the wave number increases for increasing η. Coupling strength in the full model is small: It must be on the order of 0.01 to get agreement with the phase models. Stronger coupling results in only synchronous dynamics.

C. Antiwaves in chains of coupled oscillators

Antiwaves have been studied by Ermentrout and Kopell in two separate publications [17,27]. The previous mechanisms for generating antiwaves rely on extremely long chains (essentially infinite) or chains with distal connections.

Assuming an isotropic chain with no gradient in the natural frequencies, the intermediate stable phase-locked state defined by $H(\phi^*)_{\text{odd}} = 0$ will generate traveling waves. If the fixed point ϕ^* is identified as the wave number k, then the one kink antiwave solution can be written

$$\phi_j = kj + \omega t, \quad j < j^*, \qquad \phi_j = -kj + \omega t, \quad j \geqslant j^*. \tag{19}$$

In these equations j^* represents the position of the kink. By substituting the above expression into (15), we see again that the antiwave is a solution provided that $H(k) = H(-k)$ [k is the root of $H_{\text{odd}}(k)$]. Figure 3 demonstrates examples of antiwaves obtained in the Wang-Buszaki model compared with a phase model. Figures 3(a) and 3(c) are waves generated in the full model with nonperiodic and nonreflecting boundary conditions, respectively. Figures 3(b) and 3(d) are the equivalent phase models.

D. Obtaining different wave solutions from random initial conditions

In order to see the variety of antiwaves, we will start chains of oscillators with random initial phases to estimate the basins of attraction [28]. The interaction function we use (11) allows any number of shocks or kinks in the antiwave, constrained only by the length of the chain. However, if we start the equations from random initial conditions, the probability of getting a certain number of shocks varies as we change the size of the Fourier components. The main point is that even if the odd portion of the interaction function allows for a multiple shock solution, the probability of the system converging to this solution from random initial conditions may be extremely low and is determined by the magnitude of both the even and first odd Fourier modes. Figure 4 shows the probability

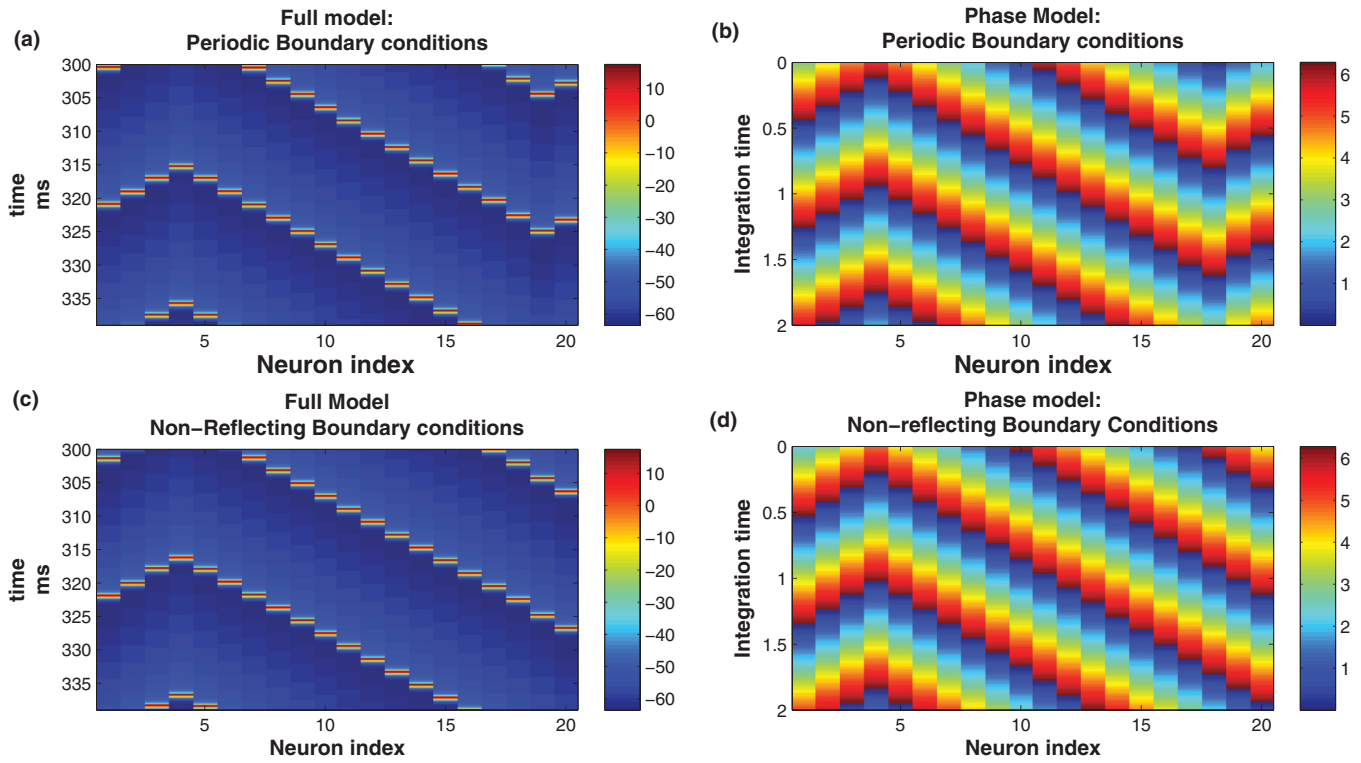

FIG. 3. (Color online) Four examples of antiwaves in both rings and chains of oscillators computed with $\eta = 6.0$. (a) is a wave in a chain of Wang-Buszaki neurons with periodic boundary conditions. (b) is a wave in a chain of phase oscillators with periodic boundary conditions. (c) is a wave in a ring of Wang-Buszaki neurons with nonreflecting boundary conditions (full model). (d) is the phase model reduction of (c): It is a wave in a chain of phase oscillators with nonreflecting boundary conditions.

distributions of obtaining various antiwave and traveling wave solutions as a function of the magnitudes of both the even and odd Fourier terms of the interaction function. Figure 4(a) is a plot of the probability of obtaining either an N-shock antiwave solution or a traveling wave (0-shock) solution as a function of a_1. From the plot, we see that the probability of obtaining a traveling wave solution approaches zero as $a_1 \to 0$ and the probability distribution shifts towards $N = 6$. As a_1 increases towards 1, the probability of obtaining the traveling wave solution increases until it is the most probable state. Figure 4(b) is a plot of the probability distribution as a function of b_1 with $a_1 = 1$. Figure 4(b) shows a trend similar to Fig. 4(a). For $b_1 = 0$ the probability of obtaining a traveling wave solution from random initial conditions is close to 0. The solution with the maximal probability corresponds to an antiwave with $N = 9$ shocks or kinks. As b_1 is increased towards 1 or decreased towards -1, the probability distribution shifts towards $N = 0$. That is, solutions with fewer kinks become more probable. Figures 4(c) and 4(d) demonstrate the effect of higher order even terms. Figure 4(d) demonstrates that using the interaction function with two even terms $[H(\phi) = \cos(\phi) + b_1 \sin(\phi) - \frac{3}{4}\sin(2\phi)]$ results in a probability distribution in which the traveling wave solution is the most probable solution for $b_1 \to 1$ and the one-kink antiwave solution is the most probable for $b_1 \to -1$. If we do not include this second order term, as demonstrated in Fig. 4(c), the most probable solution corresponds to an ($N = 4$ shocks) antiwave. The main point of this is that, even though only the odd Fourier modes determine the solutions to Eqs. (13) and (15), the even Fourier modes can drastically affect the basin of attraction of those solutions.

E. Moving the shock position with impulses

Electric fish have been observed to produce complex antiwave type patterns [27]. What is more, the lead oscillator or (kink) in these antiwaves has been observed to be able to shift position. We present a mechanism which shifts the position of the shock in the antiwave without changing its shape. Over the past 15 years, Pikovsky and Rosenau have written several papers studying waves in oscillator lattices with purely even coupling. They showed that such interaction functions can be derived from networks of Josephson junctions and Van der Pol oscillators [36–38]. Waves in these networks take the form of solitary pulses which retain their shape. Pikovsky and Rosenau have coined these waves "compactons" [36–38]. Collisions between different compactons have been studied in detail. Nothing, however, has written about compactons colliding with a phase boundary (as the phase shock in the antiwave). Compactonlike pulses are possible not only in systems with a purely even interaction function, but they can be observed in systems with odd terms, provided the even component is large enough [38]. The odd portion of the interaction function acts to dissipate the initial pulse, but a compactonlike wave may still travel large distances even with a substantial odd term. Compactons are possible in systems in which the interaction function generates antiwaves. For instance, we consider a system of 200 phase-difference

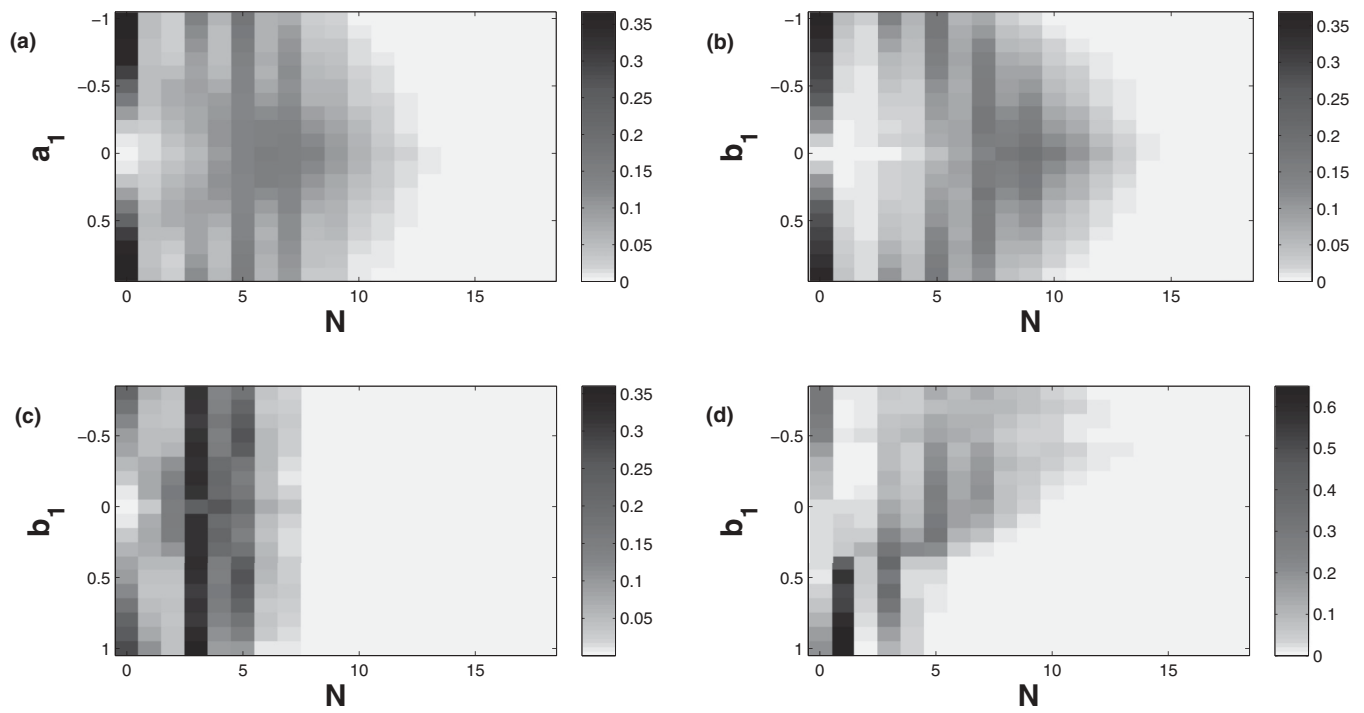

FIG. 4. Probability of obtaining different solutions of Eq. (15) for 20 oscillators as a function of the Fourier coefficients of the interaction function. N designates the number of shocks in an antiwave. $N = 0$ corresponds to a traveling wave. (a) The probability distribution with $H(\phi) = a_1 \cos(\phi) + b_1 \sin(\phi) + 0.75 \sin(2\phi)$ as a function of a_1 with $b_1 = 1$. (b) The probability distribution with $a_1 = 1$ and varying b_1. (c) The probability distribution calculated with an interaction function $H(\phi) = -3\cos(\phi) - 0.92\cos(2\phi) + b_1 \sin(\phi) - 0.75\sin(2\phi)$. (d) The probability distribution calculated using the interaction function $H(\phi) = -3\cos(\phi) + b_1 \sin(\phi) - 0.75\sin(2\phi)$. For each parameter value the equations were solved from 10 000 random initial conditions.

equations with nonreflecting boundary conditions. The interaction function used is $H(\phi) = \cos(\phi) + \sin(\phi) - 0.75\sin(2\phi)$. The initial conditions are the one-kink antiwave solution with an extra pulse stimulus applied at the end. Thus we have the one shock solution

$$\begin{aligned} \phi_j(0) &= k, \quad j < \frac{N}{2}, \\ \phi_j(0) &= -k, \quad j \geqslant \frac{N}{2}, \end{aligned} \tag{20}$$

with the addition of a pulse

$$\phi_j(0) = k + \frac{A}{2}\left(1 + \cos\left((j - x_0)\pi/\sigma\right)\right), \quad |j - x_0| < \sigma. \tag{21}$$

Here A is the amplitude, x_0 is the position of the pulse, and σ is the width of the pulse. In Fig. 5 the pulse width used is $\sigma = 10$ and $|k| = 0.841\,06$. This pulse is the form used by Pikovsky *et al.* to generate compactons, but other initial conditions may work as well [38]. Figure 5(c) shows multiple compactons traveling on top of an antiwave and colliding with the shock located at $N = 100$. The antiwave is composed of the stationary white and gray regions. The gray region of the plot corresponds to the solution $\phi = 0.841$ whereas the white region corresponds to $\phi = 5.44$. Upon collision, the shock shifts but retains its shape. In this manner, multiple pulses initiated at the ends of the chain may be used to shift the shock back and forth. Figure 5(b) is a plot of the shift in the kink as a function of the initial compacton amplitude. The maximum shift obtained is approximately nine sites. If $A > 1.5$ rad, larger amplitude pulses do not necessarily provide larger position shifts. If the pulse is too large, it will destroy the "perfect kink" solution. Thus, near the supercritical pitchfork bifurcation, not only can the shock of an antiwave form anywhere along the the chain, but precisely because of this property, it can be shifted around by an impulse (compacton). In this way, the additional even and odd Fourier terms produce a central pattern generator which is malleable. Perhaps this is a mechanism by which the hindbrain of a fish could send impulses to the rest of its spinal cord to modify the fish's swimming pattern.

IV. STABILITY ANALYSIS

In analyzing the stability of antiwave solutions, one of the main questions we want to address is how the relative contributions of each Fourier mode contribute to the stability of the solution. Additionally, we want to examine the importance of other parameters in the model, such as the length of the chain and the position of the kink. In these chain models there are four basic wave solutions which are of interest. Two of the solutions correspond to a traveling wave in either direction (left to right or right to left) and two correspond to antiwaves. The first antiwave solution describes a wave emanating from the center of the chain and propagating in both directions outward. The second antiwave solution corresponds to two

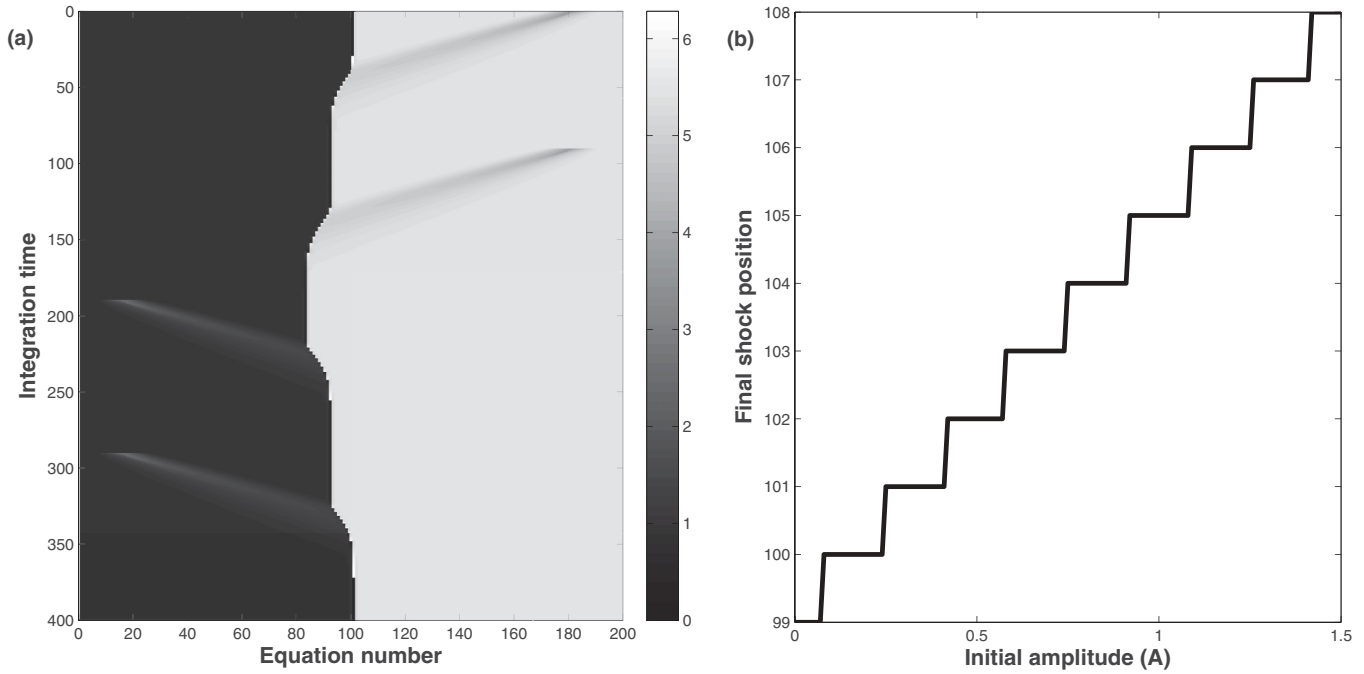

FIG. 5. (a) Compactons initiated from either side of the chain can shift the phase shock in the antiwave back and forth. The interaction function used was $H(\phi) = \cos(\phi) + \sin(\phi) - 0.75\sin(2\phi)$. (b) The shift in the kink for varying initial compacton amplitudes.

waves emanating from the edges and colliding in the center of the chain. Using our simplified interaction function we begin by analyzing the simplest (shortest) chain possible, the three-neuron system. The three phase equations (22) describing the neurons can be condensed to two by a change of variables. Linearizing these equations (23) about the antiwave solution results in a 2×2 Jacobian. Thus, the problem is simple enough so that we can solve for the eigenvalues as a function of a_1 and subsequently show where and how the antiwave solution loses stability. Once we have proved stability for this simple case, we discuss longer chains and, specifically, we analyze the effects of the magnitude of the even component on the stability of various antiwave solutions.

A. Stability analysis of the three-oscillator system

Our equations for the system with nonreflecting boundary conditions are

$$\begin{aligned} \dot{\theta}_1 &= 2H(\theta_2 - \theta_1), \\ \dot{\theta}_2 &= H(\theta_3 - \theta_2) + H(\theta_1 - \theta_2), \\ \dot{\theta}_3 &= 2H(\theta_2 - \theta_3). \end{aligned} \tag{22}$$

We then write them in terms of their phase differences:

$$\begin{aligned} \dot{\phi}_1 &= 2H(-\phi_2) - H(-\phi_1) - H(\phi_2), \\ \dot{\phi}_2 &= H(-\phi_1) + H(\phi_2) - 2H(\phi_1). \end{aligned} \tag{23}$$

Note that these equations are invariant under a reflection: $\phi_1 \to -\phi_2$, $\phi_2 \to -\phi_1$.

Figure 6 is a plot of the nullclines of the system (23) for various values of a_1 using $b_1 = 1$ and $b_2 = -0.75$. There are two antiwave solutions indicated by the boxes and two traveling wave solutions which are circled. One can see that when there is no even component the solutions to the system possess perfect reflection symmetry. As soon as a_1 is nonzero, the system loses this symmetry. We want to analyze analytically the stability of the antiwave. Choosing $\phi_1 = k$ and $\phi_2 = -k$, we linearize our equations about this system and write down the Jacobian as follows:

$$M_0 = \begin{pmatrix} H'(-k) & -2H'(k) - H'(-k) \\ -H'(-k) - 2H'(k) & H'(-k) \end{pmatrix}. \tag{24}$$

Solving for the eigenvalues of this expression, we have

$$\lambda_{1,2} = -2H'(k), \; -2H'(-k) - 2H'(k). \tag{25}$$

As long as the derivative of these H functions evaluated at this solution is positive, then the solution will be stable. Substituting the simplified interaction function (26) and its derivative into Eq. (25) results in the eigenvalue expressions, Eqs. (27):

$$\begin{aligned} H(\phi) &= b_1\sin(\phi) + b_2\sin(2\phi) + a_1\cos(\phi), \\ H'(\phi) &= b_1\cos(\phi) + 2b_2\cos(2\phi) - a_1\sin(\phi), \end{aligned} \tag{26}$$

$$\begin{aligned} \lambda_1 &= -2(b_1\cos(k) + 2b_2\cos(2k) - a_1\sin(x)), \\ \lambda_2 &= -4(b_1\cos(k) + 2b_2\cos(2k)). \end{aligned} \tag{27}$$

At the critical value of the parameter $a_{\text{critical}} = 1.1$, the first eigenvalue vanishes. For larger values of a_1, the fixed point becomes unstable. The mirror symmetry of the equations, along with the bifurcation diagram in Fig. 6, suggest that this is a subcritcal pitchfork bifurcation. This is verified in Ref. [39], where we explicitly calculate the normal form equations.

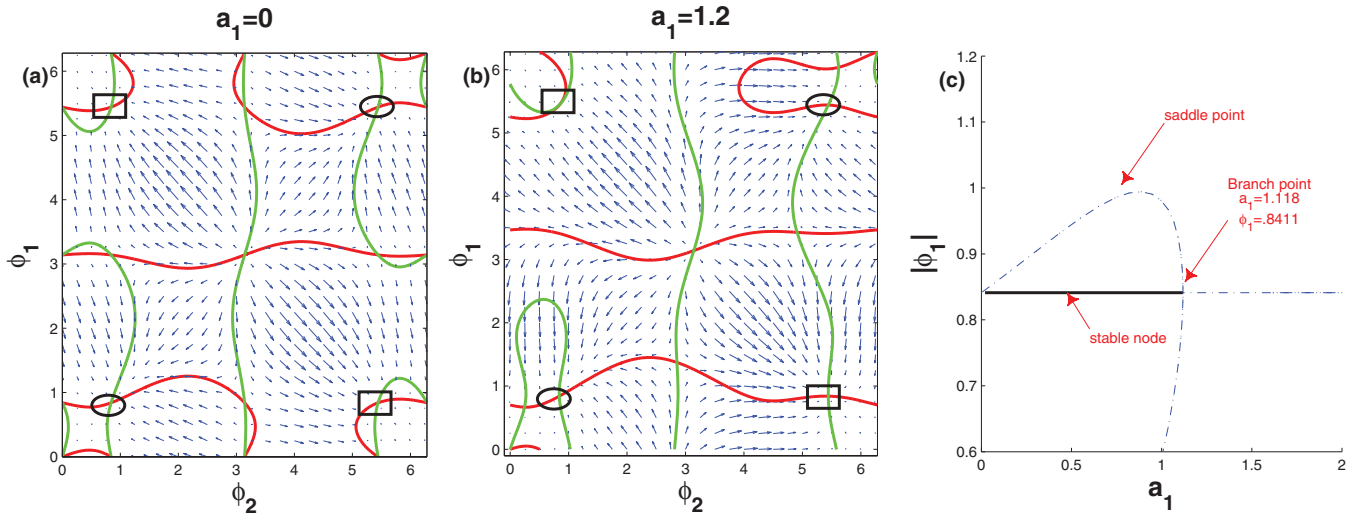

FIG. 6. (Color online) Phase portrait of the two-dimensional system (23), where $H(\phi) = a_1 \cos(\phi) + \sin\phi - 0.75 \sin 2\phi$. The ϕ_1 (ϕ_2) nullcline is in red/gray (green/light gray). (a) The nullclines and the flow for $a_1 = 0$. The fixed points corresponding to antiwaves are enclosed with boxes. The fixed points corresponding to traveling waves are circled. (b) The nullclines and the flow for $a_1 = 1.2$. (c) Bifurcation diagram computed with auto: The antiwave solution loses stability near $a_1 = 1.118$. In this plot, the stable solution is represented by a solid line whereas the unstable solution is represented by the dotted lines.

B. Stability analysis for the traveling wave

Proving the stability of the traveling wave (with no kinks) is relatively straightforward. We begin by writing down the equations for the "jth" oscillator. Since the system employs nearest-neighbor coupling, the general expression is

$$\dot{\phi_j} = H(\phi_{j+1}) + H(-\phi_j) - H(-\phi_{j-1}) - H(\phi_j). \quad (28)$$

Defining $a = H'(\phi^*)$, $b = H'(-\phi^*)$, and linearizing the equations about the wave solution, the equations for the phase are simply a discretized version of Laplace's equation

$$a\phi_{j+1} - (a+b)\phi_j + b\phi_{j-1} = \lambda\phi_j. \quad (29)$$

We may solve for the equations by assuming a general solution

$$\phi_j = Ax_1^j + Bx_2^j, \quad (30)$$

and invoking the boundary conditions $\phi_0 = \phi_1$ and $\phi_{N-1} = \phi_N$. Plugging our solution (30) into (29), we may solve for the eigenvalues of the system:

$$\mathrm{Re}\,\lambda = 2\sqrt{ba}\cos\frac{\pi m}{N-1} - (a+b). \quad (31)$$

Therefore the wave solution will always be stable provided that

$$2\sqrt{ba} \leqslant a+b, \quad (32)$$

or alternately that $a,b > 0$. Stability is lost for $a,b < 0$.

C. Stability for the antiwave under more general conditions

Stability analysis of the antiwave solutions may be proven using a combination of the Gershgorin circle theorem and numerically computing the eigenvalues of the linearized equations. In these examples, we use nonreflecting boundary conditions. The argument will be identical for periodic boundary conditions. One starts by assuming a one-shock solution and linearizing the phase the equations about this solution. The Jacobian will have matrix elements of the form

$$\begin{aligned} a_{i,i} &= -[H'(\phi_j) + H'(\phi_j)], \quad a_{i,i+1} = H'(\phi_{j+1}), \\ a_{i,i-1} &= H'(\phi_{j-1}). \end{aligned} \quad (33)$$

All other matrix elements are zero. Once more, define $a = H'(\phi^*)$, $b = H'(-\phi^*)$. If l denotes the location of the kink, then the matrix elements corresponding to the kink are

$$a_{l,l} = -(a+b), \quad a_{l,l+1} = b, \quad a_{l,l-1} = b, \quad (34)$$

or

$$a_{l,l} = -(a+b), \quad a_{l,l+1} = a, \quad a_{l,l-1} = a, \quad (35)$$

depending on the orientation of the shock. The Gershgorin circle theorem [40] tells us that all of the eigenvalues of the matrix lie in the union of disks centered at the diagonal elements of the matrix with radii less than the absolute value of the sum of the row entries not including the diagonal terms. If the Jacobian of the antiwave is described by Eq. (34), all eigenvalues will lie in the union of three disks: one centered at $-(a+b)$ with radius $a+b$, one centered at $-2a+b$ (corresponding to the ends of the chain) with radius a, and one centered at $-(a+b)$ with radius $2b$. If we assume that the even term a_1 is positive and increasing, then $H'(-\phi) \geqslant H'(\phi)$,

$$\begin{aligned} |b| &\geqslant |a|, \\ |2b| &> |a+b|. \end{aligned} \quad (36)$$

Thus the disks will extend beyond the origin, and we will not be able to say anything about stability using this theorem. On the other hand, if the solution is a shock oriented in the opposite direction, such as in Eq. (35), the disk corresponding to the equation at the shock is centered at $-(a+b)$ and extends out with radius $|2a|$. The disk will always lie in the left

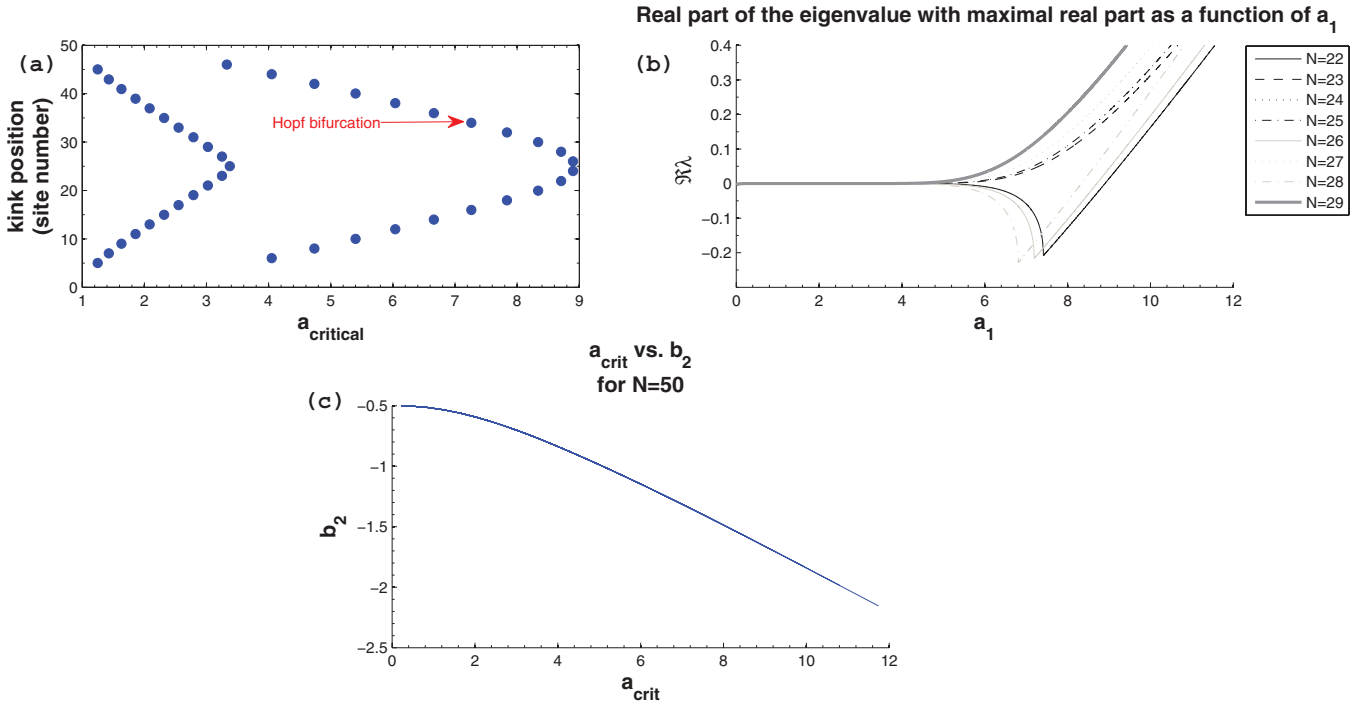

FIG. 7. (Color online) (a) Critical value of a_1 as a function of shock position. (b) Eigenvalue with the maximal real part as a function of a_1 for different shock positions. N denotes the location of the shock. (c) An interaction function with a more negative b_2 can also possess a larger a_1 before the solution becomes unstable.

half of the imaginary plane for a_1 positive. Therefore, this solution will always be stable. In the former case, in which the fractured wave is not necessarily stable, one must apply numerical methods to explicitly calculate the eigenvalues of the Jacobian. We are interested in how variables such as the position of the shock and the length of the chain affect the stability of the solution as we vary the magnitude of the first even Fourier mode. Again, we use the interaction function $H(\phi) = b_1 \sin(\phi) + b_2 \sin(2\phi) + a_1 \cos(\phi)$, where $b_1 = 1$ and $b_2 = -0.75$. We start by examining a 51-oscillator chain (described by 50 equations) in which we move the position of the shock. Figure 7(a) shows the critical value of a_1 at which the shock solution loses stability as a function of shock position where the position varies between site 4 and site 46. The parameter a_{critical} is determined by calculating the eigenvalues of the Jacobian for various values of a_1 and determining when the eigenvalue with the maximal real part becomes positive. Figure 7(b) plots the real part of the eigenvalue with a maximal real part as a function of a_1: As the position shifts, the eigenvalues lose stability at different values of a_1. The type of bifurcation by which they lose stability changes as well. For shocks located at even numbered sites, the system loses stability in a Hopf bifurcation as a complex conjugate pair of eigenvalues crosses the origin simultaneously. For shocks located at odd sites the system apparently loses stability in a subcritical pitchfork bifurcation (this has not been rigorously proven). Figure 7(c) is a plot of a_{critical} for the eigenvalues of the 51-oscillator Jacobian linearized about solutions corresponding to varying values of b_2. The plot clearly demonstrates that shock solutions corresponding to a larger value of b_2 can support a larger even component before becoming unstable. Figure 8 is a plot of a_{critical} versus the number of phase-difference equations (number of oscillators in a chain). The shock is always located centrally, e.g., for 101 oscillators, the shock is located at $N = 50$. For an odd number of phase-difference equations, the shock position is obtained by dividing the number of equations in half and rounding up. Figure 8 shows phenomena similar to Fig. 10(a). That is, a solution will lose stability for different a_1 dependent on the position of the shock in the solution as well as the number of oscillators in the chain. In the case that the shock is perfectly centered, we expect the solution to lose stability in a subcritical pitchfork. Regardless of the position of the shock, even for relatively short chains the antiwave solution will be stable for a relatively large even component, whose magnitude is at least as large as the first odd Fourier mode. The manner in which the solution loses stability and the size of the even component it can support depend on both the position of the shock and the length of the chain. The Gershgorin circle theorem tells us that one of the antiwave solutions will always be stable, no matter how long the chain.

V. PATTERN FORMATION IN TWO-DIMENSIONAL ARRAYS

Antiwave patterns can be observed in two-dimensional networks as well. Using nearest-neighbor coupling, the differential equation for a single oscillator is

$$\frac{d\theta_{x,y}}{dt} = H(\theta_{x+1,y} - \theta_{x,y}) + H(\theta_{x,y+1} - \theta_{x,y}) + H(\theta_{x,y-1} - \theta_{x,y}) + H(\theta_{x-1,y} - \theta_{x,y}), \quad (37)$$

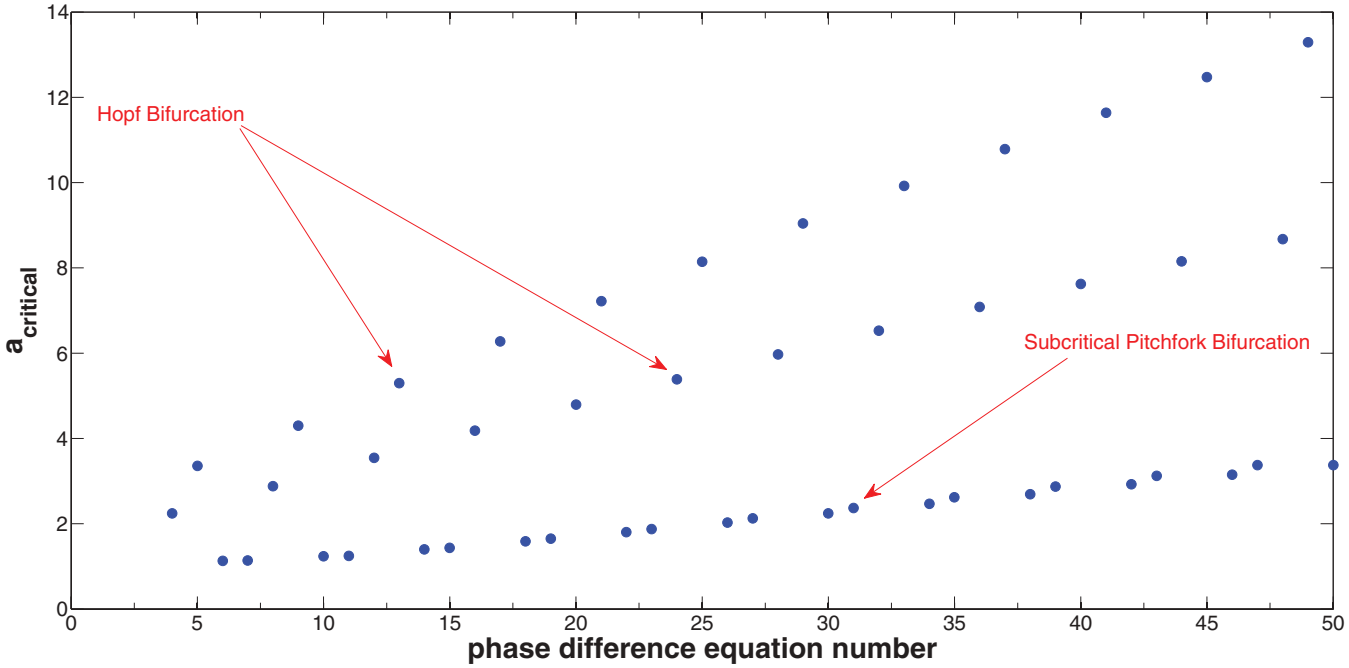

FIG. 8. (Color online) Critical value of a_1 as a function of chain length where N represents the number of phase-difference equations ϕ_N. Depending on the length of the chain and position of the shock, the solution may lose stability in either a Hopf bifurcation or what is believed to be a subcritical pitchfork bifurcation. The shock is always located centrally (e.g., for 101 oscillators, the shock is located at $N = 50$. For an odd number of phase-difference equations, the shock's position is obtained by dividing the number of equations by half and rounding up.)

where x, y are discrete indices describing the location of an oscillator. These indices run from 1 to N, where N^2 is the number of differential equations in the array. As in the one-dimensional case, we use nonreflecting boundary conditions. Examples of these patterns and the interaction functions used to generate them are illustrated in Fig. 9. Figures 9(b)–9(d) are stationary and numerically stable. Figure 9(b) is generated from random initial conditions. Figures 9(c) and 9(d) are stable

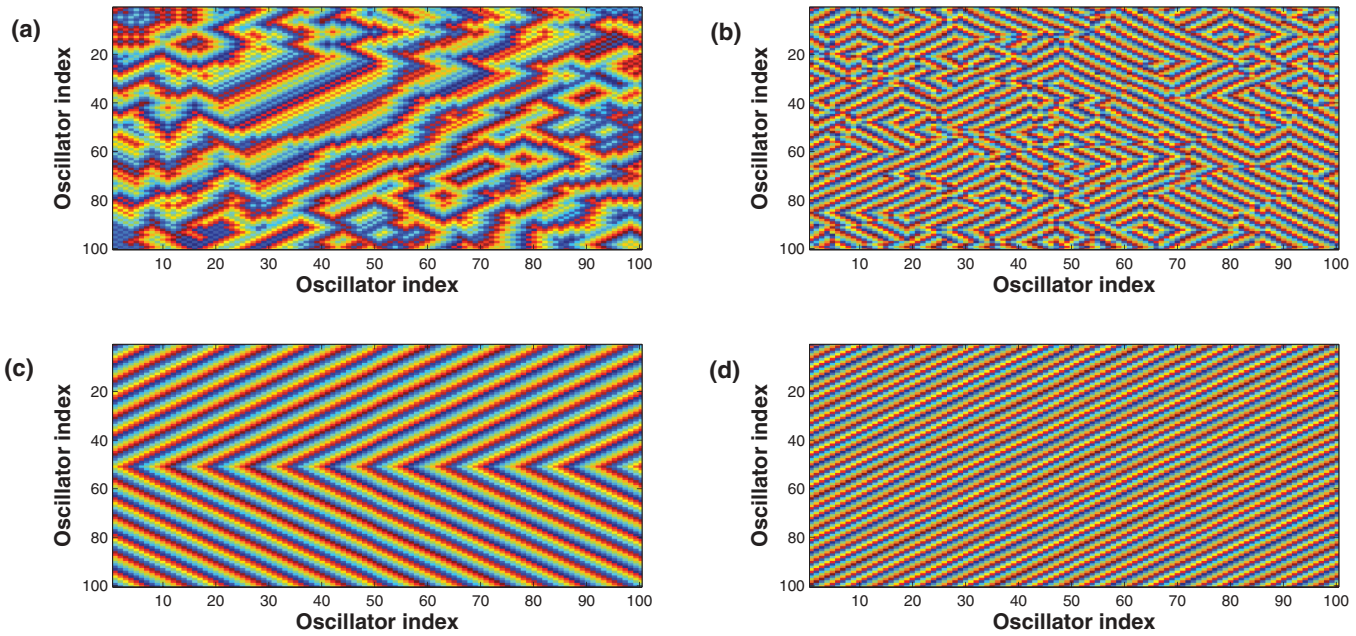

FIG. 9. (Color online) Examples of two-dimensional patterns. The horizontal and vertical axes are the oscillator indices. (a) Snapshot of a slowly varying wave pattern obtained from compactonlike initial conditions: A two-dimensional pulse is initiated in the upper left-hand corner of the array on a synchronous background. The interaction function used is $H(\phi) = \sin(\phi) - \cos(\phi) - 0.75\sin(2\phi)$. (b) Stable stationary fractured pattern obtained from random initial conditions and interaction function $-2\cos(\phi) - 0.518\sin(\phi) - 1.31\sin(2\phi) - 0.933\sin(3\phi)$. (c) Stationary antiwave generated with $H(\phi) = \cos(\phi) + \sin(\phi) - 0.75\sin(2\phi)$. (d) Stationary traveling wave generated with the same interaction function as (c).

but have a very small basin of attraction. The initial conditions must be almost identical to the actual antiwave or traveling wave solution.

Analogous to the one-dimensional case, a plane wave may be represented by the solution

$$\theta_{xy} = k_x x + k_y y + \omega t, \tag{38}$$

whereas the shock solution may be written

$$\begin{aligned} \theta_{xy} &= k_x x + k_y y, \quad x \leqslant x^*, \\ \theta_{xy} &= -k_x x + k_y y, \quad x > x^*. \end{aligned} \tag{39}$$

In these equations x^* is the location of the shock. A shock may be thought of as a discontinuous boundary between the two traveling waves. The fractured pattern in Fig. 9(b) is composed of many small waves of varying k_x and k_y which form shocks. Fractured patterns are generated with random initial conditions where the phases are chosen between 0 and 2π [41,42].

VI. CONCLUSION

Intermediate stable phase-locked states occur in a variety of neuron models and are capable of producing a pattern of wavelike activity known as an antiwave. This type of activity was first observed in the dogfish spinal cord by Grillner [32] and it may occur in other networks as well [12,33]. The mechanism we use for generating these waves may have an experimental basis: Peinado *et al*. have shown that modulating the potassium conductance of gap-junction-coupled neurons in the neonatal mouse neocortex leads to wave behavior [13]. The mechanism for generating traveling waves and antiwaves is more flexible than past models, because it allows one to modulate the wavelength of the wave by adjusting properties such as the potassium conductance or temperature-dependent time constant. It allows for a huge variety of phase-locked patterns in a chain or array of neurons. In the case of antiwave generation, it does not require distal connections and the shock can form anywhere along the chain. The shock position can also be moved by colliding phase compactons. This may provide a mechanism by which an animal such as the dogfish could switch between different swimming patterns. More generally, near the bifurcation from in-phase synchrony, the interaction functions of the phase model have large higher order Fourier modes. This is in contrast to many oscillator models that were used in the past, which only include the lowest odd Fourier mode. The odd modes determine the value of the stable-phase locked solution but the even modes affect the stability of the antiwave solution. Varying the relative even component affects the basin of attraction of a particular solution, or the probability that the phases will converge to a particular antiwave solution from random initial conditions. Finally, we note that this behavior is not only relevant to chains but to two-dimensional arrays as well.

APPENDIX: THE WANG-BUSZAKI MODEL

The parameters used in the Wang-Buszaki model are $v_{\rm syn} = -60.5$ mV, $g_L = 0.1$ mS, $v_L = -65$ mV, $g_{\rm Na} = 35$ mS/cm^2, $V_{\rm Na} = 55$ mV, $g_{\rm K} = 9$ mS/cm^2, $V_{\rm K} = -90$ mV, $a_{i0} = 4$, $\tau_i = 15$ ms, and $i_0 = 0.63$ nA/cm^2. The nonlinearites mentioned in Sec. II A are given by the following expressions:

$$\begin{aligned} &\alpha_m(V) = 0.1(V + 35.0)/(1.0 - \exp(-(V + 35.0)/10.0)), \\ &\beta_m(V) = 4.0\exp(-(V + 60.0)/18.0), \\ &M_\infty(V) = \alpha_m(V)/(\alpha_m(V) + \beta_m(V)), \\ &\alpha_h(V) = 0.07\exp(-(V + 58.0)/20.0), \\ &\beta_h(V) = 1.0/(1.0 + \exp(-(V + 28.0)/10.0)), \\ &H_\infty(V) = \alpha_h(V)/(\alpha_h(V) + \beta_h(V)), \\ &\alpha_n(V) = 0.01(V + 34.0)/(1.0 - \exp(-(V + 34.0)/10.00)), \\ &\beta_n(V) = 0.125\exp(-(V + 44.0)/80.0), \\ &N_\infty(V) = \alpha_n(V)/(\alpha_n(V) + \beta_n(V)). \end{aligned} \tag{A1}$$

[1] S. Grillner, Science **228**, 143 (1985).
[2] E. Izhikevich, *Dynamical Systems in Neuroscience: The Geometry of Excitabilty and Bursting* (MIT Press, Cambridge, MA, 2007).
[3] G. Buzsáki and A. Draguhn, Science **304**, 1926 (2004).
[4] A. H. Cohen, P. J. Holmes, and R. H. Rand, J. Math. Biol. **13**, 345 (1982).
[5] B. Ermentrout, J. Flores, and A. Gelperin, J. Neurophysiol. **79**, 2677 (1998).
[6] B. Ermentrout, M. Pascal, and B. Gutkin, Neural Comput. **13**, 1285 (2001).
[7] J. G. Mancilla, T. J. Lewis, D. J. Pinto, J. Rinzel, and B. W. Connors, J. Neurosci. **27**, 2058 (2007).
[8] C. Vreeswijk, L. F. Abbott, and G. Bard Ermentrout, J. Comput. Neurosci. **1**, 313 (1994).
[9] A silicon neuron refers to an electronic circuit designed to mimic a biological neuron.
[10] G. S. Cymbalyuk, G. N. Patel, R. L. Calabrese, S. P. DeWeerth, and A. H. Cohen, Neural Comput. **12**, 2259 (2000).
[11] A. Gelperin, J. Exp. Biol. **202**, 1855 (1999).
[12] U. Kim, T. Bal, and D. A. McCormick, J. Neurophysiol. **74**, 1301 (1995).
[13] A. Peinado, J. Neurophysiol. **85**, 620 (2001).
[14] G. Ermentrout and D. Kleinfeld, Neuron **29**, 33 (2001).
[15] Y. Momose-Sato, K. Sato, and M. Kinoshita, Eur. J. Neurosci. **25**, 929 (2007).
[16] G. B. Ermentrout and D. Terman, *Mathematical Foundations of Neuroscience* (Springer, Berlin, 2012).
[17] N. Kopell and G. B. Ermentrout, Commun. Pure Appl. Math. **39**, 623 (1986).
[18] P. C. Bressloff, S. Coombes, and B. de Souza, Phys. Rev. Lett. **79**, 2791 (1997).
[19] S. Jones, B. Mulloney, T. Kaper, and N. Kopell, J. Neurosci. **23**, 3457 (2003).
[20] G. B. Xiao-Jing Wang, J. Neurosci. **16**, 6402 (1996).
[21] $\eta = Q_{10}^{T-T_{\rm base}}$: In this equation, Q_{10} is the "ratio of the rates for an increase in temperature of 10 °C" [16].
[22] B. Pfeuty, G. Mato, D. Golomb, and D. Hansel, J. Neurosci. **23**, 6280 (2003).

[23] M. P. Nusbaum and M. P. Beenhakker, Nature (London) **417**, 343 (2002).
[24] S. P. Javedan, R. S. Fisher, H. G. Eder, K. Smith, and J. Wu, Epilepsia **46**, 574 (2002).
[25] S. H. and Strogatz, Physica D **143**, 1 (2000).
[26] H. Haken, J. Kelso, and H. Bunz, Biol. Cybern. **51**, 347 (1985).
[27] G. B. Ermentrout and N. Kopell, SIAM J. Appl. Math. **54**, 478 (1994).
[28] D. A. Wiley, S. H. Strogatz, and M. Girvan, Chaos **16**, 015103 (2006).
[29] B. Blasius and R. Tönjes, Phys. Rev. Lett. **95**, 084101 (2005).
[30] These are not to be confused with fractured waves studied by Kopell (also known as *s* waves) [43].
[31] B. Denardo, B. Galvin, A. Greenfield, A. Larraza, S. Putterman, and W. Wright, Phys. Rev. Lett. **68**, 1730 (1992).
[32] S. Grillner, Exp. Brain Res. **20**, 459 (1974).
[33] J. Christensen and R. L. Hauser, Am. J. Physiol. **221**, 1033 (1971).
[34] K. W. Thompson, J. Comput. Phys. **68**, 1 (1987).
[35] To see that this is consistent with the preceding statement, start with the $H(-\phi_{j-1}) = H(\phi_j)$, then, using a Taylor series to expand out each side and evaluating at the wave solution, we have the expression

$$H'(-\phi)\frac{d\phi}{dx} = 0.$$

Since $H'(-\phi) \neq 0$, then it must be that $(\frac{d\phi}{dx}|_{x=0}) = 0$.
[36] A. Pikovsky and P. Rosenau, Physica D **218**, 56 (2006).
[37] K. Ahnert and A. Pikovsky, Phys. Rev. E **79**, 026209 (2009).
[38] K. Ahnert and A. Pikovsky, Chaos **18**, 037118 (2008).
[39] A. Urban, Ph.D. thesis, University of Pittsburgh, 2011.
[40] Gershgorin circle theorem: Let $A = [a_{ij}]$ be an arbitrary $n \times n$ matrix with elements that may be complex and let

$$\Lambda_i = \sum_{j=1, i\neq j}^{n} |a_{ij}| \quad \text{for} \quad i = 1,2,\ldots,n.$$

Then all of the eigenvalues λ_i of A lie in the union of n disks Γ_i where

$$\Gamma_i : |\lambda - a_{ii}| \leqslant \lambda_i \quad \text{for} \quad i = 1,2,\ldots,n.$$

This wording of the Gershgorin circle theorem was taken from Ref. [44].
[41] All equations in this section were integrated with Euler's method. The step size used is 0.01.
[42] The Fourier terms used may or may not be calculated from the full model. For instance, an interaction function with an artificially inflated second odd mode will produce an interesting fractured pattern, whereas many interaction functions computed from the full model will not.
[43] D. Somers and N. Kopell, Physica D **89**, 169 (1995).
[44] I. Gradshteyn and I. Ryzhik, *Tables of Integrals, Series and Products* (Academic Press, San Diego, 2000).